Cheng *et al. Cell Communication and Signaling* (2025) 23:474
https://doi.org/10.1186/s12964-025-02478-4

Cell Communication and Signaling

RESEARCH Open Access

Müller glia-mediated protection of retinal ganglion cells from ethambutol-induced neurotoxicity through brain-derived neurotrophic factor

Hui-Chen Cheng[1,2], Yu-Hui Wong[3,4†], An-Guor Wang[1,2†], Shih-Wei Chen[4], Yong-Lin Yang[4], Hsien-Chia Juan[4,5], Roxanne Hsiang-Chi Liou[4] and Jenn-Yah Yu[3,4*†]

Abstract

Background Ethambutol (EMB)-associated optic neuropathy is the most common toxic optic neuropathy and poses a significant visual threat worldwide. This study aimed to investigate the neuroprotective roles of Müller glia, the most abundant macroglia in the retina, and their associated growth factors in supporting retinal ganglion cells (RGCs) under EMB-induced toxicity.

Methods Induced RGC-like cells (iRGCs), differentiated from human induced pluripotent stem cells, and Müller glial cell line MIO-M1 were used as cellular models. The response of iRGCs to EMB was investigated by using RNA sequencing. A transwell co-culture system was used to evaluate the protective effect of MIO-M1 cells on iRGC survival. Candidate trophic factors from MIO-M1 cells were measured by using quantitative RT-PCR. Brain-derived neurotrophic factor (BDNF) was identified as the major factor contributing to the neuroprotective effect from Müller glia. The effect of BDNF was further validated in both iRGCs and mouse retinal organotypic culture under EMB toxicity. Downstream signals of the BDNF pathway were investigated by Western blot.

Results RNA sequencing revealed that EMB significantly disrupted neurotrophins and BDNF-associated pathways in iRGCs. Co-culture with MIO-M1 cells markedly enhanced the survival of iRGCs during EMB exposure. mRNA of BDNF and nerve growth factor (NGF) were elevated in MIO-M1 cells, while only BDNF improved the survival and morphological integrity of iRGCs under EMB treatment. Administration of BDNF also improved the survival of RGC in mouse retinal explants. The pro-survival effect of BDNF was suppressed by GNF5837, a pan-TRK inhibitor. Among the three downstream effectors of BDNF signaling, AKT was most prominently activated by BDNF in EMB-treated iRGCs, compared to ERK and PLCγ1. Furthermore, the protective effect of BDNF was blocked by the AKT inhibitor MK-2206 but not by the ERK inhibitor GDC-0094.

†Yu-Hui Wong, An-Guor Wang and Jenn-Yah Yu contributed equally to this work.

*Correspondence:
Jenn-Yah Yu
jyyu@nycu.edu.tw

Full list of author information is available at the end of the article

© The Author(s) 2025. **Open Access** This article is licensed under a Creative Commons Attribution-NonCommercial-NoDerivatives 4.0 International License, which permits any non-commercial use, sharing, distribution and reproduction in any medium or format, as long as you give appropriate credit to the original author(s) and the source, provide a link to the Creative Commons licence, and indicate if you modified the licensed material. You do not have permission under this licence to share adapted material derived from this article or parts of it. The images or other third party material in this article are included in the article's Creative Commons licence, unless indicated otherwise in a credit line to the material. If material is not included in the article's Creative Commons licence and your intended use is not permitted by statutory regulation or exceeds the permitted use, you will need to obtain permission directly from the copyright holder. To view a copy of this licence, visit http://creativecommons.org/licenses/by-nc-nd/4.0/.

Conclusions Müller glia confer neuroprotection to RGCs under EMB-induced stress, primarily via BDNF signaling. AKT functions as the key downstream effector mediating this protective response. These findings suggest that the BDNF-AKT signaling may serve as a promising therapeutic target for EMB-associated optic neuropathy.

Keywords Brain-derived neurotrophic factor, Ethambutol, Müller glia, Optic neuropathy, Retinal ganglion cell

Background

Ethambutol (EMB) is a first-line antiobiotic for the treatment of tuberculosis and other *Mycobacterium avium* complex infections [1]. There are about 9.2 million new cases of tuberculosis each year according to an estimation from World Health Organization, which means a significant number of patients will be receiving EMB treatment at one time or another [1]. However, optic neuropathy is a major adverse event of EMB treatment and may lead to irreversible visual loss [2]. With an incidence of 1% to 5%, EMB-induced optic neuropathy may account for 100,000 or more new cases each year and is the most common toxic optic neuropathy in the world [1, 2]. Advanced age, hypertension, and renal disease are recognized risk factors for EMB-associated optic neuropathy [3].

The exact mechanism underlying EMB-induced optic neuropathy remains unknown [4]. Several mechanisms have been proposed to contribute to its pathogenesis. As a metal chelator, EMB may disrupt mitochondrial function and oxidative phosphorylation by interfering with iron-containing complex I and copper-containing complex IV [5, 6]. In addition, EMB may inhibit lysosomal activation, leading to zinc accumulation in lysosomes, which increases lysosomal membrane permeability and ultimately causes cell death [7]. Autophagy dysregulation has also been noted as occurring during EMB-related optic neuroretinopathy [8]. However, an efficacious treatment for EMB-induced optic neuropathy is still not available. There is an unmet need for managing EMB-related optic neuropathy, especially considering the significant number of individuals affected worldwide.

Glial cells, which account for approximately 90% of cells in the brain, have been found to play a more significant role than previously thought [9]. In addition to acting as a structural support for neurons, glial cells also have functions such as extracellular matrix generation, volume regulation, metabolism, regulating neuronal activity, synaptic pruning, gliosis, phagocytosis, neuroprotection and even neural regeneration [9]. Glial cells are usually activated in a disease state and when there is disturbance to cell homeostasis; in this context glial cells, may either protect neurons or trigger the death of residual neurons [9]. For examples, in a model of glaucoma, glial cells release neurotrophic factors that help neurons to overcome the insult. On the other hand, up-regulation of TNF-α/TNFR signaling, NF-κB activation, p53 and caspase 3 have also been noted in optic nerve head astrocytes [10]. Pathogenic glial dysfunction has been proposed to be involved in age-related macular degeneration and retinitis pigmentosa [11, 12]. Thus, the microenvironment built up by glial cells may play an important role in modulating neuronal survival. In the retina, there are three main kinds of glial cells, namely Müller cells, astrocytes and microglia. Among them, Müller cells are specialized glial cells, whose processes span the entire thickness between the internal and external limiting membrane, and are key factor in the structural, metabolic, homeostatic, and functional support of retinal cells [13–15].

In order to explore the neuroprotective solutions in EMB-related optic neuropathy, we hypothesize that Müller glia, the most abundant macroglia in the retina, may play a protective role in retinal ganglion cells (RGC) that are suffering from EMB toxicity. We used RGC-like cells (iRGCs), differentiated from human induced pluripotent stem cells (hiPSCs), as our in vitro model. The reprogrammed iRGCs have been shown to express various RGC-specific markers and electrical properties, which means they can be a representative model for the study of optic neuropathy [16]. We first studied EMB toxicity in iRGCs by using RNA sequencing. Subsequently, the effect of Müller cell co-culture on the survival of iRGCs under EMB toxicity was investigated. The potential trophic factors secreted by EMB-treated Müller glia was also studied. Candidate factors were tested for their ability to enhance iRGC survival, and the associated molecular pathways were explored. Finally, key findings from the cellular model were verified in the mouse retinal organotypic culture system.

Methods

Culturing MIO-M1 cells

The human Müller cell line Moorfields/Institute of Ophthalmology- Müller 1 (MIO-M1) is a spontaneously immortalized human Müller glia cell line and was obtained from the UCL Institute of Ophthalmology, London, UK [17]. MIO-M1 cells were maintained in high glucose (4 gram/liter) Dulbecco's Modified Eagle Medium (DMEM, Gibco) supplemented with 10% fetal bovine serum (FBS, Gibco) and 100 U/ml penicillin, 100 U/ml streptomycin and 4 mM glutamine in humidified incubator with an atmosphere of 5% CO_2 at 37 °C.

Culture of human induced pluripotent stem cells (hiPSCs) and differentiation of RGC-like cells (iRGCs)

The hiPSC lines, NTUH-iPSC-01–05 and NTUH-iPSC-02-02 (abbreviated as N1 and N2, respectively), were purchased from Bioresource Collection and Research Center of Food Industry Research and Development Institute, Taiwan. The use of these hiPSC lines followed the Policy Instructions of the Ethics of Human Embryo and Embryonic Stem Cell Research guidelines in Taiwan. Furthermore, approval from the Institutional Review Boards of National Yang Ming Chiao Tung University was obtained (# NYCU112122AW). Human iPSCs were routinely maintained in StemFlex medium (Gibco) on vitronectin-coated (Gibco) dishes at 37°C in a 5% CO_2 incubator following the manufacturer's instructions. Passage of the cells was performed when the culture reached 80% to 90% confluence, which typically occurred every 5 days. A passaging ratio of 1:10 was used.

To generate retinal ganglion cells (iRGCs), hiPSCs were first transduced with lentiviruses carrying the ATOH7, BRN3B, and SOX4 genes under the control of a Tet-on expression system [16]. For iRGC differentiation, the infected hiPSCs were seeded at 70% confluency. On the following day, designated as day 0, the differentiation process was initiated by adding 2 μg/mL of doxycycline. The cells were then cultured in Medium-1, which consisted of DMEM/F12 (Gibco) supplemented with N-2 (Gibco), non-essential amino acids (NEAA, Gibco), 200 ng/mL mouse laminin (Gibco), 10 ng/mL brain-derived neurotrophic factor (BDNF, PeproTech), 10 ng/mL ciliary neurotrophic factor (CNTF, PeproTech), 10 ng/mL basic fibroblast growth factor (bFGF, PeproTech), and 5 μM forskolin (Sigma-Aldrich). On day 1, Medium-1 was replaced and 1 μg/mL puromycin and 2 μg/mL zeocin were added to allow selection of successfully induced cells. Puromycin selection was maintained for 24 h, while zeocin selection continued until day 6. On day 2, the cells were dissociated using 0.5 mM EDTA and then replated onto culture plates coated with poly-L-lysine and laminin. These cells were then cultured in Medium-2, a combination of DMEM/F12 and Neurobasal (1:1) supplemented with N-2, B-27 (Gibco), GlutaMAX (Gibco), 200 ng/mL mouse laminin (Gibco), 10 ng/mL BDNF, 10 ng/mL CNTF, 10 ng/mL bFGF, 5 μM forskolin, 2 μg/mL of doxycycline, and 2 μg/mL zeocin. On day 4, Medium-2 was refreshed with the addition of 2.5 μM arabinofuranosyl cytidine (AraC) to inhibit the proliferation of undifferentiated cells. On day 6, after 48 h of AraC treatment, Medium-2 was replaced with Medium-3, which consisted of Neurobasal supplemented with N-2, B-27, and GlutaMAX, along with supplementary substances including 200 ng/mL mouse laminin, 10 ng/mL BDNF, 10 ng/mL CNTF, 10 ng/mL bFGF, and 5 μM forskolin. Hereafter, the cells were cultured in Medium-3, with half-medium changes occurring every 3–4 days until day 20, at which point the cells were utilized for downstream applications (Figure S1).

Cell viability assay using alamarBlue®

Culture medium was replaced by fresh medium containing 10% (v/v) alamarBlue® (Thermo Fisher Scientific) and the cells were incubated at 37 °C in a 5% CO2 incubator for 2 to 4 h. AlamarBlue® contains resazurin, which is reduced by metabolically active cells to resorufin, a red, highly fluorescent product. Viable cells sustain this process, leading to increased fluorescence and intensification of the surrounding media's color. After the color of the medium turned pink, fluorescence was measured at excitation/emission wavelengths of 560/590 nm using a TECAN Infinite 200. The negative control was defined as fluorescence from the wells containing no cells, treated in the same manner. Cell viability was calculated as followed: cell number index (%) = (mean reads of the sample – mean reads of the negative controls)/(mean reads of the sample without EMB treatment – mean reads of the negative controls).

Animal handling and ethics statement

Seven-week-old wild-type male C57BL/6 mice (24–28 g, BioLASCO Taipei, Taiwan) were used in this study. All procedures regarding animal handling and euthanizing complied with the ARVO Statement for the Use of Animals in Ophthalmic and Vision Research and were approved by the Institutional Animal Care and Use Committee (IACUC) of Taipei Veterans General Hospital and of National Yang Ming Chiao Tung University. No randomization was used due to the nature of study design. No blinding was done in this study. If applicable, at least 3 batches of independent experiments were done to ensure the reproducibility of the data.

Preparation of mouse retinal organotypic culture

Adult mice are euthanized by carbon dioxide (CO_2) overdose and confirmed to be dead based on cardiac arrest and fixed dilated pupils. Retinal explant culture followed the established protocols with some modifications [18]. Peritomy was done and the eyeball was enucleated. The cornea was then removed, followed by expelling the lens and removing the iris. After a radial cutting of the sclera, the retina was carefully separated from underlying retinal pigment epithelium and sclera. The retina was then transferred to the culture insert, with the photoreceptor layer facing the track etched polycarbonate membrane (TEPC), pore size 0.4 μm and 25 mm in diameter (Whatman) at the bottom of insert. The retina was then cut at the 3, 6, 9, and 12 o'clock positions and carefully flattened using blunt-end forceps. The retina was maintained in basic culture medium with or without EMB in

an incubator with a humidified atmosphere and 5% CO_2 at 37 °C for 24 h. The culture medium was a composite made of Neurobasal-A, with N-2 (Gibco), B-27 supplement (Gibco), and antibiotics (100 μg/ml streptomycin and 100 units/ml penicillin (Gibco).

Live/dead viability assay

For the visualization of cell viability, the LIVE/DEAD® Viability/Cytotoxicity Kit (Thermo Fisher Scientific), which is based on plasma membrane integrity and esterase activity, was performed according to the manufacturer's instructions. Live cells with ubiquitous intracellular esterase activity can convert the nonfluorescent cell-permeant calcein AM into the fluorescent calcein, which can be observed at excitation/emission wave lengths of 495/515nm. Ethidium homodimer-1 (EthD-1) can penetrate damaged membranes and become fluorescent at excitation/emission wavelengths of495/635nm after binding to nucleic acids. The live cell ratio was defined as the number of live cells/number of live and dead cells within a 300 × 300 μm area from each sample; this was assessed using a fluorescence microscope (Olympus IX83). The cell size was calculated as the total area of live cells in Live/Dead viability assay over the number of live cells in the entire field, to quantify the degree of cellular swelling.

Immunofluorescence microscopy

The iRGCs were cultured on coverslips and subjected to immunofluorescence. Cells were fixed with 4% paraformaldehyde in phosphate-buffered saline (PBS) for 15 min, and then permeabilized with 0.2% Triton X-100 in PBS for 15 min at room temperature. The cells were then blocked with 3% bovine serum albumin in PBS for 60 min at room temperature. Primary antibodies in the blocking solution were added to the cells and they were then incubated overnight at 4 °C. After removing the primary antibodies and rinsing, secondary antibodies in blocking solution, together with 4', 6-diamidino-2-phenylindole (DAPI, 1 μg/ml), were added for 1 h at room temperature. The antibodies and dilutions used in this study are listed in Table S1. After washing, the coverslips were mounted in the Fluoromount-G solution (Invitrogen). The fluorescent images were acquired using an Olympus IX83 inverted microscope. Neurites were visualized using MAP2 immunostaining, which primarily labels dendritic processes. Neurite length was measured using the NeurphologyJ plugin integrated with ImageJ [19]. Neurite length per cell was calculated by dividing the total neurite length within the field of view by the number of cells.

Confocal microscopy

The retinas were transferred to the slides carefully and subjected to immunofluorescence. The retinal flat mounts were fixed with 4% paraformaldehyde in PBS for 20 min. After washing with 0.1% Triton X-100 in PBS for 30 min for 3 times, the retinas were heated at temperatures greater than 95 °C in 10 mM sodium citrate buffer (pH 6.0) for 20 min, and then permeabilized with 0.2% Triton X-100 in PBS for 20 min at room temperature. The retinas were then blocked with 5% bovine serum albumin in PBS for 60 min at room temperature. Primary antibodies in the blocking solution were added and incubated overnight at 4 °C. After removing the primary antibodies and rinsing, matched secondary antibodies in blocking solution were added for 2 h at room temperature. The retinas were then incubated with 1 μg/ml DAPI for 30 min at room temperature for nuclear staining, which was followed by washing with PBS for 5 min 5 times. The retinal flat mounts were mounted with antifade medium (Vectashield HardSet H1400, Vector Laboratories) and images were taken using a confocal microscope (Zeiss LSM700). The antibodies and dilutions used in this study are listed in Table S1. The samples with poor staining/imaging quality were excluded for further analysis.

RNA extraction and real-time quantitative PCR (quantitative RT-PCR)

Total RNA was extracted from MIO-M1 cells using a Total RNA Mini Kit (Geneaid Biotech) according to the manufacturer's instructions. The RNA was reverse transcribed to cDNA using the SuperScript IV Reverse Transcriptase (Thermo Fisher Scientific) reaction. The cDNA was used for RT-qPCR, which was performed on an ABI StepOne™ real-time PCR machine using TaqMan™ Master Mix (Roche).

The threshold crossing value was observed for each transcript, which was then normalized against the corresponding control (MIO-M1 cells without EMB treatment) and internal control (TATA-box binding protein (TBP)). The comparative CT method was used for the relative quantification of mRNA. The data were processed on StepOnePlus Real-Time PCR Systems (Thermo Fisher Scientific). The sequences of the probes and primers used were listed in Table S2.

Protein extraction and Western blot

Cells and mouse retinal samples were lysed with RIPA lysis buffer, which consisted of 50 mM Tris-HCl (pH 7.4), 150 mM NaCl, 1% IGEPAL CA-630, 0.5% Sodium deoxycholate, 0.1% SDS, 2 mM EDTA, and 50 mM NaF, supplemented with EDTA-free proteinase inhibitor cocktail (Roche). The protein concentrations were measured using a BCA Protein Assay Kit (Thermo Fisher Scientific). Finally, the cell lysates were denatured at 85 °C for 10 min.

Next, the proteins were separated on an 12% SDS-PAGE gel at 100 V for 2 h in running buffer (25 mM

Tris, 190 mM glycine, 0.1% SDS). The gels were then transferred to PVDF membranes by electrophoresis at 80 V for 2.5 h in transfer buffer (25 mM Tris, 190 mM glycine, 20% methanol). The membranes were blocked with 5% skimmed milk in TBST (25 mM Tris, 150 mM NaCl, 0.05% Tween-20) for 30 min and then probed with primary antibody at 4 °C overnight. After washing with TBST, the membranes were incubated with horseradish peroxidase (HRP)-conjugated matched secondary antibodies at room temperature for 1 h. Thereafter, the secondary antibodies were washed out and the signals were visualized by Immobilon Western Chemiluminescent HRP Substrate (Millipore). Densitometric analysis of the bands was performed using ImageJ.

Messenger RNA library constructing and sequencing

Total RNA was extracted from day 21 iRGCs treated with 1000 μg/mL ethambutol (Sigma-Aldrich) or vehicle (PBS) using RNA Mini Kit (Geneaid). The mRNA library construction and sequencing were performed by Azenta Life Sciences company. For library preparation, 1 μg of total RNA was used. The poly(A) mRNA was isolated using Oligo(dT) beads. The mRNA fragmentation was achieved using divalent cations and high temperature. Priming was performed using Random Primers. First strand cDNA and the second-strand cDNA were synthesized. The purified double-stranded cDNA was then treated to repair both ends and add a dA-tailing in one reaction, followed by a T-A ligation to add adaptors to both ends. Size selection of adaptor-ligated DNA was then performed using DNA Clean Beads. Each sample was then amplified by PCR using P5 and P7 primers, and the PCR products were validated. Libraries with different indices were multiplexed and loaded on an Illumina NovaSeq 6000 system for sequencing using a 2 × 150 paired-end (PE) configuration according to manufacturer's instructions.

Bioinformatics workflow

The reads in fastq format underwent quality filtering (score ≥ Q15, qualified percentage > 60%) and adapter trimming using fastp (version 0.20.1). The remaining reads were mapped to Human Genome Reference GRCh38 using STAR (version 2.7.5a) to generate output in the BAM file format. Expected counts and transcripts per million (TPM) were then computed using RSEM (version 1.3.1). Downstream analysis of the expected counts was performed in R Statistical Software (version 4.2.1; R Core Team 2022) using DESeq2 package (version 1.36.0). Variance stabilizing transformation and differential gene expression (DEG) analysis were performed using vst and DEseq in DESeq2 package. Variance stabilized read counts were used to perform principal component analysis (PCA). Differentially expressed genes (DEGs), comparing EMB-treated to vehicle- treated iRGCs, were defined by an adjusted p-value < 0.05 and a fold change > 1.5. Under these criteria, 683 genes were identified as up-regulated DEGs, and 374 genes were identified as down-regulated DEGs. These DEGs were then analyzed using QIAGEN Ingenuity Pathway Analysis (version 111725566). Plots were created using Python (version 3.8.17) with matplotlib (version 3.7.1). The RNA-seq data discussed in this publication have been deposited in NCBI's Gene Expression Omnibus and are accessible through GEO Series accession number GSE294687 (https://www.ncbi.nlm.nih.gov/geo/query/acc.cgi?acc=GSE294687).

Statistical analysis

The distribution of the data was tested by Shapiro-Wilk test to check if the data is within normal distribution. Student's t-test was used for continuous variables with normal distribution and Kolmogorov-Smirnov test was used while the continuous variables were not normally distributed. Analysis of variance (ANOVA) followed by multiple comparisons test was performed among the different experimental groups to allow inter- and intragroup analysis. If the data were not normally distributed, Kruskal-Wallis test with Dunn's multiple comparisons test was performed instead. All analysis were performed by using GraphPad Prism version 10.1.1 for macOS (GraphPad Software). A $p < 0.05$ (two-sided) was defined as statistically significant. The p values of group comparisons that attained statistically significance were listed in Table S3.

Results

EMB-induced cytotoxicity on human induced pluripotent stem cell-derived retinal ganglion cells (iRGCs)

In order to investigate EMB-induced optic neuropathy, we used iRGCs derived from human iPSCs as our model (Fig. 1). After administering EMB onto iRGCs for 24 h at the indicated concentrations, we observed significant changes in cell morphology. At EMB concentrations above 4 mM, the iRGCs exhibited signs of swelling and an overall increase in size compared to the vehicle-treated controls (Fig. 1b, S2a and S2b). In addition, neurites, which are the elongated projections from the iRGCs, appeared to be fragmented or disrupted (Fig. 1c). Immunofluorescence staining revealed that MAP2 signals became shortened or even lost, while TUJ1 staining appeared more punctate, reflecting dot-like TUJ1-positive cell debris. This may be attributed to the relative stability of βIII-tubulin (stained by TUJ1) under stress conditions (Fig. 1c). Evidence of cellular disruption and compromised membrane integrity was further supported by the increase in the numbers of EthD-1-positive (red) dead cells and a concomitant decrease in the number of calcein-positive (green) live cells (Fig. 1b and S2a). These observations suggest that EMB treatment has a

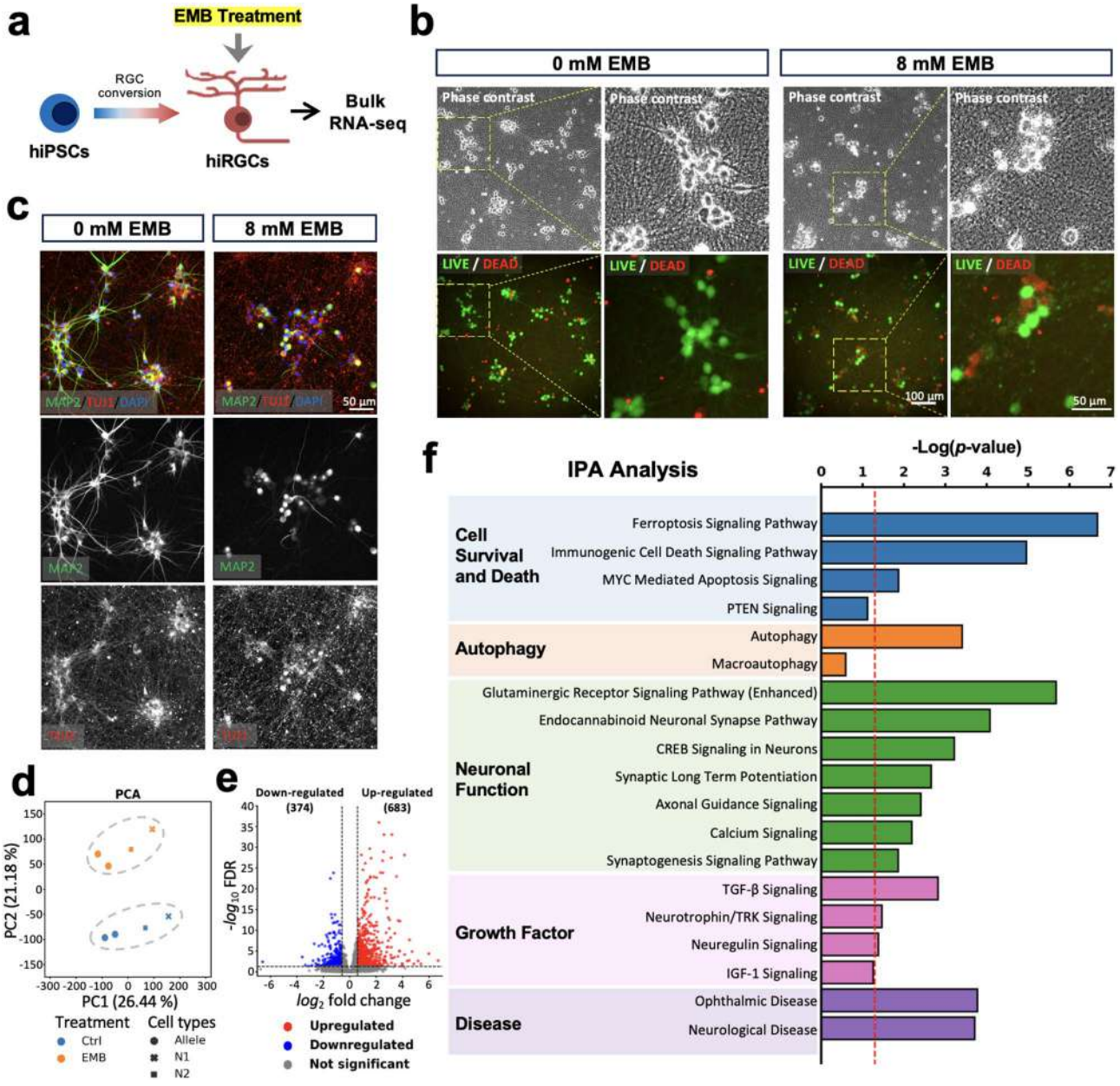


Fig. 1 Ethambutol (EMB)-induced cytotoxicity on human induced pluripotent stem cell-derived retinal ganglion cells (iRGCs). **a** Schematic representation of the experimental workflow. Human iPSCs were differentiated into iRGCs and treated with 0 mM or 8 mM EMB, followed by immunocytochemistry or RNA sequencing. **b** Phase contrast and LIVE/DEAD staining images of iRGCs treated with vehicle or 8 mM EMB, illustrating the viability of cells under different treatment conditions. iRGCs exhibited signs of swelling, with an overall increase in size compared to the control (0 mM) group. There is evidence of cellular disruption and loss of cellular integrity, indicated by an increase in EthD-1 positive (red) dead cells, and a notable decrease in the number of calcein-positive (green) live cells. Scale bar: 100 μm and 50 μm. **c** Immunofluorescence images showed the expression of neuronal markers TUJ1 (red) and MAP2 (green) in iRGCs treated with vehicle or 8 mM EMB. The neurites, which are the elongated projections of iRGCs, appear fragmented or disrupted under EMB toxicity. Scale bar: 50 μm **d** Principal component analysis (PCA) plot of transcriptomic data of vehicle or EMB-treated iRGCs ($n = 4$ biological replicates from 3 hiPSC lines). **e** Volcano plot showing differentially expressed genes (DEGs) in hiRGCs treated with 8 mM EMB versus vehicle (fold change > 1.5 and FDR < 0.05). **f** Ingenuity pathway analysis (IPA) identifying the top enriched pathways in EMB-treated iRGCs. Categories include cell survival, autophagy, neuronal function, growth factors, and disease relevance

detrimental effect on both the morphology and viability of the iRGCs.

To further understand the molecular response of iRGCs to EMB treatment, we performed RNA sequencing on iRGCs treated with vehicle or 8 mM EMB for 24 h. Principal component analysis (PCA) plot of all transcriptomic data demonstrated distinct clustering of samples from vehicle or EMB-treated iRGCs (Fig. 1d). A total of

1057 differentially expressed genes (DEGs) were identified, including 683 up-regulated and 374 down-regulated genes (EMB vs. Vehicle; fold change > 1.5; FDR < 0.05) (Fig. 1e). Ingenuity pathway analysis (IPA) revealed several enriched pathways impacted by EMB treatment, including those related to cell survival and death, autophagy, neuronal function, growth factors, and disease relevance (Fig. 1f).

Although BDNF mRNA levels were not significantly altered following EMB treatment (Fig. 2a), NTRK2 (TrkB), the primary receptor mediating BDNF signaling, was significantly downregulated. IPA further identified the neurotrophin/Trk and CREB signaling pathways as being significantly affected (Fig. 2b), and analysis of second messengers associated with BDNF signaling showed dysregulation following EMB treatment (Fig. 2c). To examine downstream signaling, we assessed the activation of protein kinase B (AKT), extracellular signal-regulated kinase (ERK), and phospholipase C-γ1 (PLCγ1) based on their phosphorylation levels. We observed a concentration-dependent decrease in the phospho-AKT (pAKT)/AKT ratio. Phospho-ERK42/ERK42 levels decreased significantly in iRGCs treated by 4 mM and 16 mM EMB compared to the untreated group. Prominent reduction of p-PLCγ1/PLCγ1 was also noted in iRGCs treated by 16 mM EMB (Fig. 2d-h). Taken together, these findings suggest that EMB disrupts neurotrophin signaling not at the level of BDNF transcription, but through

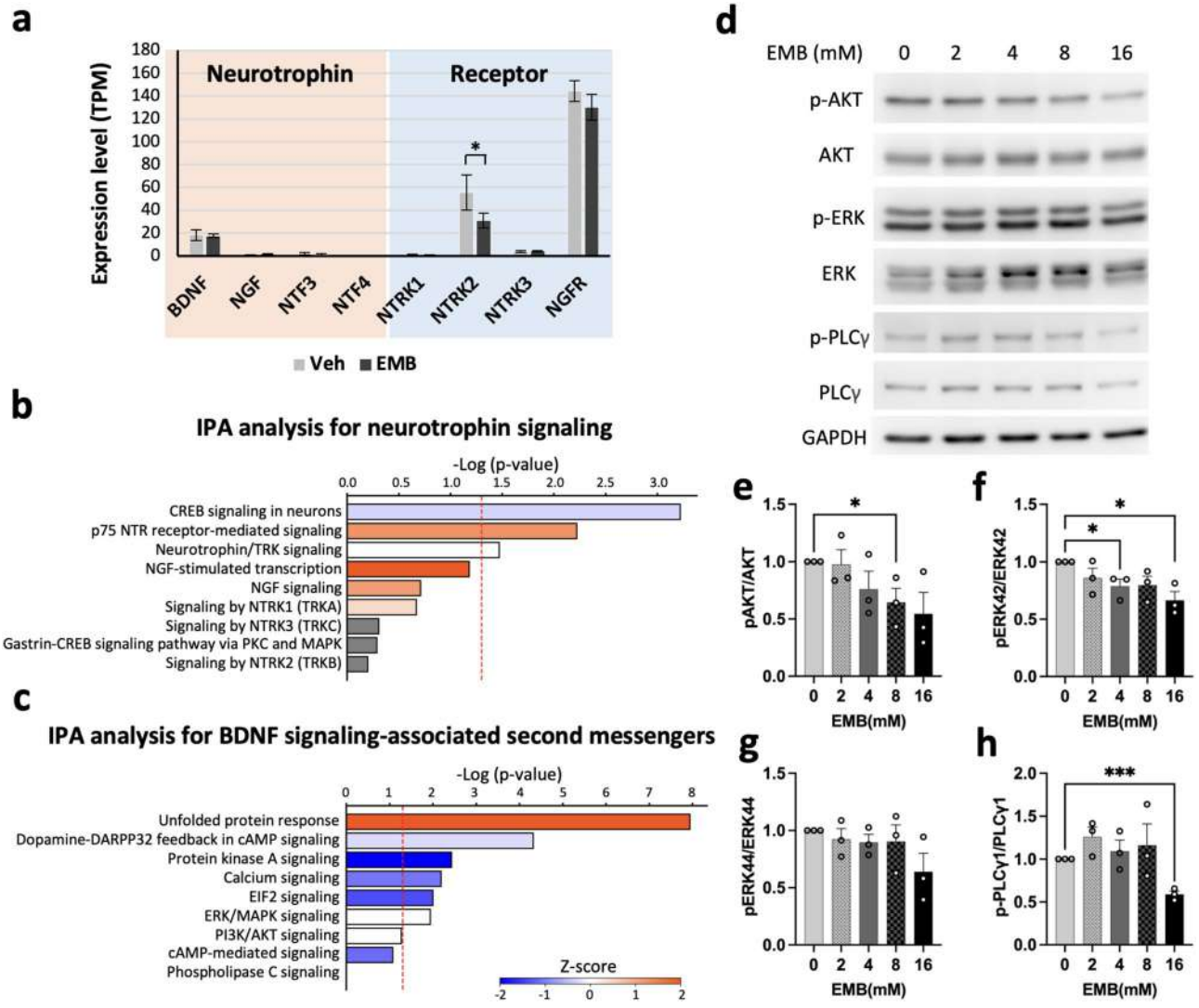


Fig. 2 Disruption of neurotrophin signaling pathway in iRGCs following EMB treatment. **a** Expression levels of neurotrophins (BDNF, NGF, NT-3, NT-4) and their receptors (NTRK1, NTRK2/TRKB, NTRK3, NGFR) in iRGCs treated with EMB or vehicle ($n = 4$ biological replicates from 3 hiPSC lines; *$p < 0.05$ by t test). **b**-**c** IPA of neurotrophin signaling (**b**) and BDNF-associated second messenger pathway (**c**) in iRGCs treated with 8 mM EMB compared to vehicle. **d** Western blot analysis of BDNF pathway-related proteins in iRGCs across different EMB concentrations for 24 h. **e**-**h** Quantification of the protein levels in (**d**). Data are presented as means ± SEM ($n = 3$ batches of independent experiments; *$p < 0.05$, *** $p < 0.001$ by t test)

downregulation of its receptor (NTRK2) and impairment of downstream signaling components. This receptor-level and post-receptor signaling dysfunction supports our hypothesis that EMB interferes with BDNF-associated neurotrophic support in iRGCs.

Co-culture of MIO-M1 cells promotes the survival of iRGCs under EMB treatment

Unlike many in vitro culture systems where RGCs or RGC-like cells are grown alone, RGCs in vivo are enveloped by Müller processes in the retina [9]. Müller cells, the principal macroglia of the retina, are essential for maintaining the structural and functional integrity of retinal neurons. It is possible that Müller cells play a role in EMB-induced optic neuropathy, so we included the human Müller cell line MIO-M1 in our study. We examined EMB-induced cytotoxicity on MIO-M1 cells first. Administration of EMB to MIO-M1 cells led to swelling, vacuole changes, an increase in the number of EthD-1 positive (red) dead cells and a decrease in the number of calcein-positive (green) live cells (Figure S2a). Cell viability was further accessed using the alamarBlue® assay. As expected, the cell number of iRGCs was decreased in parallel with the increase in EMB concentration and this occurred in a dose-dependent manner (Figure S2c). In contrast, the cell number of MIO-M1 cells remained relatively stable until 16 mM EMB was reached when there was a significant drop in cell numbers; this indicated that MIO-M1 cells are more resistant to EMB toxicity when compared to iRGCs (Figure S2c).

Next, we co-cultured iRGCs with MIO-M1 cells in a transwell co-culture system (Fig. 3a). Interestingly, co-culture of iRGCs with MIO-M1 cells in the presence of EMB reduced iRGC death (Fig. 3b and c), which suggests that Müller cells serve a protective role. Addition of culture media 30 min prior to EMB treatment also resulted in improved survival of iRGCs. However, this increase in survival was not as great as when iRGCs were directly co-cultured with MIO-M1 cells (Fig. 3b and c). Based on the cell number index, as assessed by the alamarBlue® assay, co-culturing of iRGCs with MIO-M1 cells clearly increased the cell number of iRGCs significantly across a range of EMB concentrations (Figure S3a).

Exploring the potential growth factors released by MIO-M1 cells that are able to enhance iRGC survival during EMB exposure

Various growth factors had been identified as being involved in neuroprotection when there is an optic nerve disorder [20]. To identify potential growth factors released by the MIO-M1 cells that are able to promote the survival of iRGCs, we checked the expression in MIO-M1 cells, after treatment with different concentrations of EMB, of various growth factors, namely brain-derived neurotrophic factor (BDNF), nerve growth factor (NGF), insulin-like growth factor 1 (IGF-1) and basic fibroblast growth factor (bFGF). The mRNA level of BDNF showed an approximately two-fold increase after EMB treatment at 2 mM (Fig. 4a). The mRNA level of NGF was also increased in a similar manner when the EMB concentrations increased. The mRNA level of IGF-1 was found to decrease after EMB treatment, while that of bFGF showed no change after EMB treatment. Thus, BDNF and/or NGF may act as pro-survival factors when released from Müller glial cells.

To verify the pro-survival effect of BDNF and NGF, we evaluated their effects on EMB-treated iRGCs. Administration of BDNF to iRGC cells that have been treated with 8 mM EMB resulted in improvement in iRGC morphological integrity. Live/dead staining revealed a notable increase in the percentage of live cells in the BDNF-treated group compared to the control (Fig. 4d). Although administration of NGF led to a slight increase in the cell number index at the highest concentration of EMB (8 mM), it did not improve morphology based on the microscopy and live/dead staining (Fig. 4b and c, and Figure S3b). Furthermore, addition of BDNF substantially mitigated the neurite degeneration caused by EMB treatment, as shown by the increase in MAP2-positive dendrite staining (Fig. 4d and S3b). The cell number also showed a significant increase in EMB-treated iRGCs after adding BDNF (Fig. 4e). In addition, the protein level of BDNF in MIO-M1 cells showed an increase in parallel with an increase in EMB concentration up to 4 mM, which is also supported by our quantitative RT-PCR (Fig. 4f and g). Although the protein levels could be affected not only by mRNA level, but also by translational efficiency, post-transcriptional regulation, protein degradation regulation, subcellular localization of mRNA and feedback regulation, there is generally a trend of increasing BDNF mRNA and protein levels after adding EMB in MIO-M1 cells [21].

Together with RNA sequencing data, these results support the conclusion that BDNF is a key neurotrophic factor released by MIO-M1 cells in response to EMB-induced stress, contributing to the protection of iRGCs from EMB-related neurotoxicity. In addition, we speculated BDNF 50 ng/ml as the minimum effective concentration because adding BDNF 50 ng/ml can improve cell number index across all studied concentrations of EMB and improve neurite length per cell significantly. This concentration was used for the following experiments.

The effect of BDNF on the survival of iRGCs in the presence of EMB toxicity

Since BDNF protects iRGCs from EMB-induced neurotoxicity, we investigated the possible downstream signaling of BDNF when promoting the survival of iRGCs.

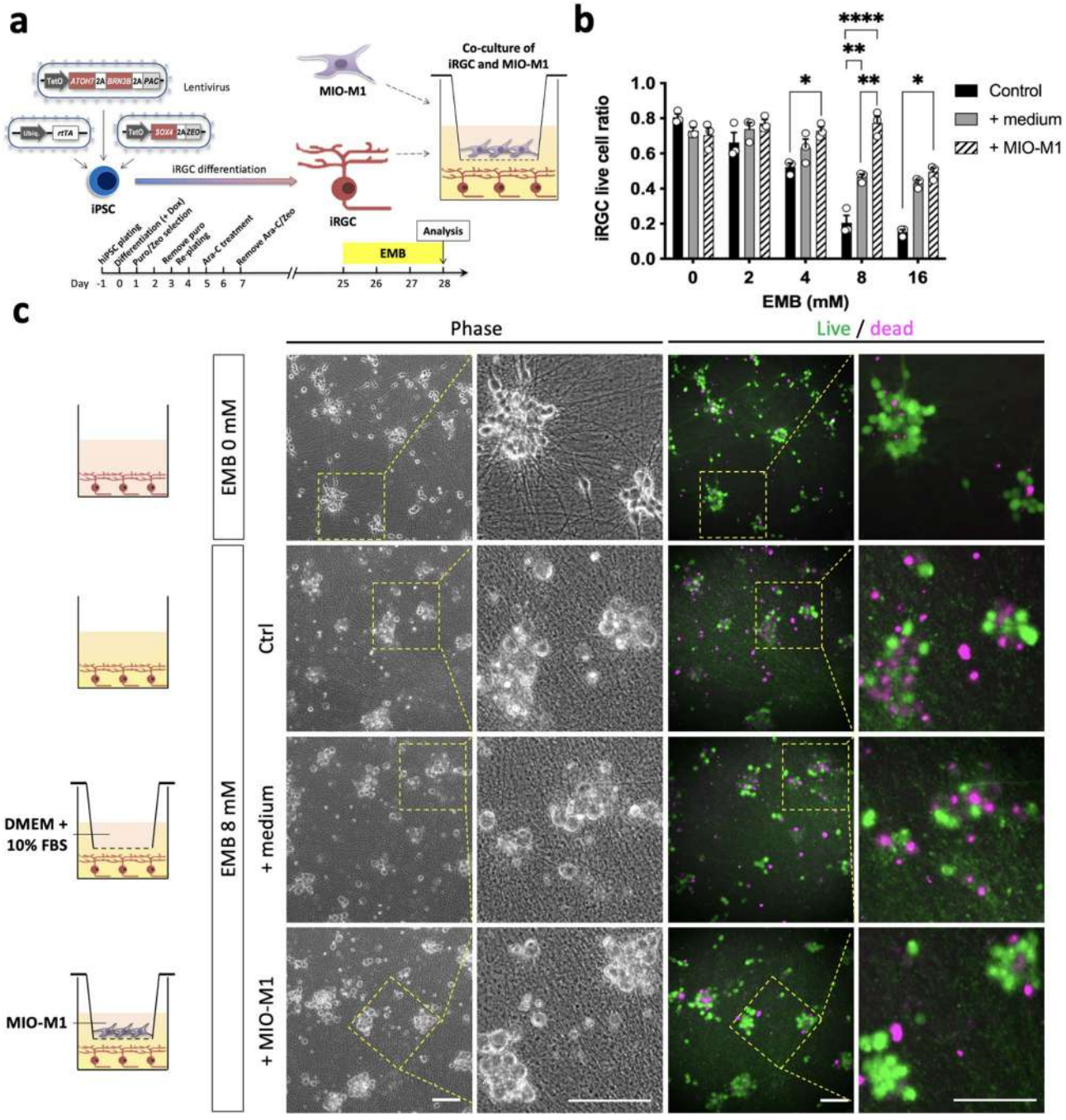


Fig. 3 Co-culture with MIO-M1 cells enhances the survival of iRGCs under EMB exposure. **a** Schematic depiction of the experimental process whereby iRGCs are co-cultured with MIO-M1 cells. At day 25, iRGCs were transferred to a transwell co-culture system and treated with different concentrations of EMB for 3 days. **b** Co-culture of iRGCs with MIO-M1 cells resulted in a significantly higher iRGC live cell ratio at EMB concentrations more than 2 mM. Adding fresh media 30 min prior to EMB treatment also improved iRGC survival, but this was not as significant as when the iRGCs were co-cultured with MIO-M1 cells. Data are presented as means ± SEM and were analyzed by Kruskal-Wallis test ($n = 3$ batches of independent experiments; *$p < 0.05$, **$p < 0.01$, ****$p < 0.0001$). **c** Co-culture of iRGCs with MIO-M1 cells in a transwell co-culture system when EMB was present reduced iRGC cell death, as indicated by the increase in calcein-positive (green) live cells and the decrease in EthD-1 positive (red) dead cells compared to control (without co-culture). Scale bar, 100 µm

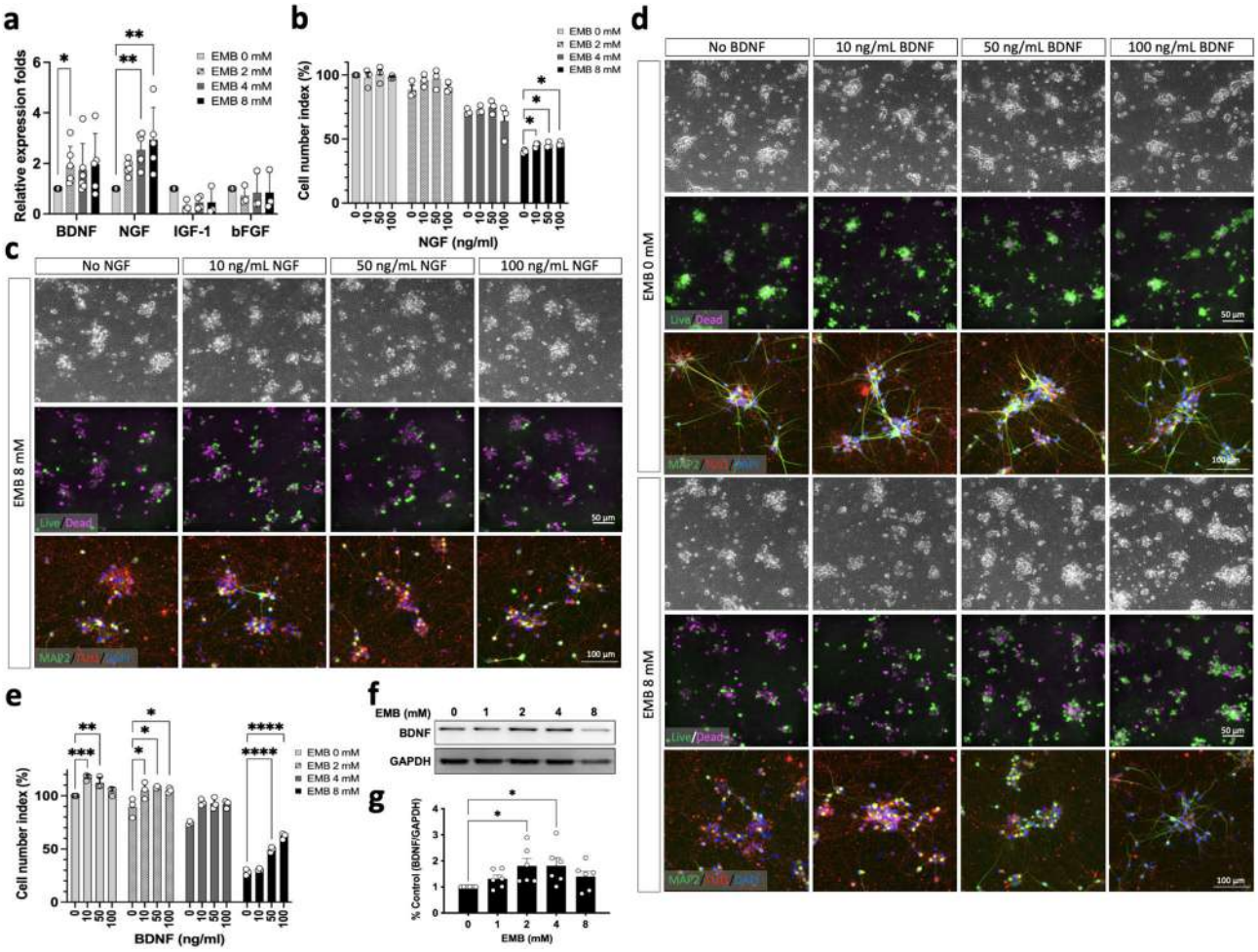


Fig. 4 Identification of the potential growth factors from MIO-M1 cells involved in iRGC protection. **a** The mRNA levels of BDNF, NGF, IGF-1 and bFGF, measured by RT-qPCR, in MIO-M1 cells treated with serial concentrations of EMB. Data are presented as means ± SEM ($n = 3$–6 batches of independent experiments; *$p < 0.05$, **$p < 0.01$ by Kruskal-Wallis test for BDNF, NGF, IGF-1; one-way ANOVA for bFGF) **b** Cell number index, measured by alamarBlue® assay, of iRGCs treated with NGF across various EMB concentrations. No significant changes were observed except at 8 mM EMB. Data are presented as means ± SEM. ($n = 3$ batches of independent experiments; *$p < 0.05$ by Kruskal-Wallis test (at EMB 1, 2, 8 mM) or one-way ANOVA (at EMB 4 mM)). **c** NGF treatment did not result in significant alterations in iRGC cell numbers and morphology. **d** BDNF treatment improved the morphological integrity of the iRGCs under 8 mM EMB, as shown by increased the live/dead ratio. Higher concentrations of BDNF led to enhanced cell survival. **e** Cell number index supports that the survival of EMB-treated iRGCs improved in the presence of BDNF. Data are presented as means ± SEM. ($n = 3$ batches of independent experiments; *$p < 0.05$, **$p < 0.01$, ***$p < 0.001$, ****$p < 0.0001$ by Kruskal-Wallis test (at EMB 1, 2, 8 mM) or one-way ANOVA (at EMB 4 mM)). f-g Western blot analysis showed an increase in BDNF protein levels in MIO-M1 cells treated with increasing concentrations of EMB (≤ 8 mM. Data are presented as means ± SEM. ($n = 6$ batches of independent experiments; *$p < 0.05$ by Kruskal-Wallis test)

BDNF has been shown to interact with receptors such as tropomyosin kinase B (TrkB) and low affinity nerve growth factor receptor (also known as p75 NTR) [26]. Inhibition of Trk with GNF-5837, a pan-Trk inhibitor, diminishes the protective effect of BDNF after EMB treatment based on the morphology of cells and of neurites, live/dead staining and immunohistochemistry (Fig. 5a and S3c). Treatment of GNF-5837 also reduced the number of BDNF treated live cells (Fig. 5a). These findings demonstrated that BDNF protects iRGCs from EMB-induced neuropathy via Trk.

AKT acts downstream of BDNF during the promoting of iRGC survival

To understand the signaling molecules contributing to the survival benefit from BDNF, we examined the phosphorylation levels of AKT, ERK, and PLCγ1 in iRGCs. The ratio of phospho-AKT (p-AKT) to total AKT increased significantly after BDNF treatment, and the effect was suppressed significantly after adding GNF5837 (Fig. 5b and c); these effects occurred both in the presence of and in the absence of EMB treatment. The ratio of phospho-ERK42 to total ERK42 decreased significantly after EMB treatment. Administration of BDNF resulted in a mild elevation in the pERK42/ERK42 ratio, although

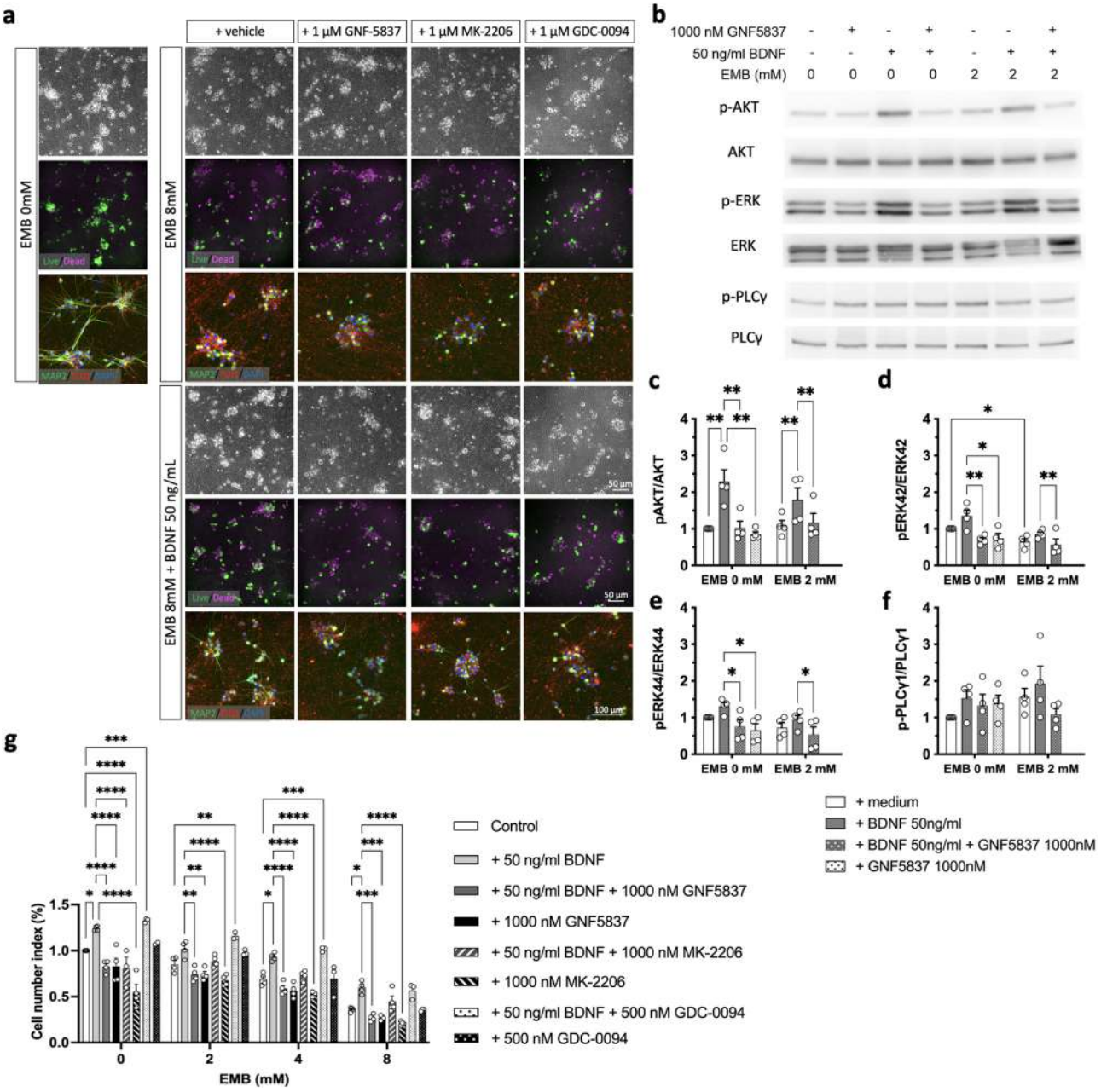


Fig. 5 The effect of BDNF on the survival of EMB-treated iRGCs and its associated signaling pathways. **a** The beneficial effect of BDNF was reduced by inhibitors that target BDNF signaling pathways, especially when the inhibitor GNF-5837 is used. **b** Western blot analysis of BDNF associated signaling pathways in iRGCs. **c**-**f** Quantification of the protein expression levels in (**b**). **c** The p-AKT/AKT ratio is increased significantly after BDNF treatment, and this effect was suppressed by GNF-5837 with or without EMB treatment ($n=4$ batches of independent experiments). **d** The pERK42/ERK42 levels are decreased significantly in the presence of EMB. The addition of BDNF resulted in a small increase, though not statistically significant ($n=4$ batches of independent experiments). **e** A similar non-significant trend was observed in the ERK44 pathway ($n=4$ batches of independent experiments). **f** The PLCγ1 pathway activity show high variability, and no consistent effect was observed ($n=4$ batches of independent experiments). **g** The cell viability accessed by alamarBlue® assay showed that BDNF improved the survival of iRGCs under various concentrations of EMB. This effect was abolished by the addition of GNF-5837 and partially suppressed by the addition of MK-2206, while GDC-0094 had no effect. GNF-5837 and MK-2206 showed similar suppression effects on the survival benefit of BDNF in iRGCs without EMB treatment. Adding MK-2206 itself resulted in a significant impact on iRGCs without EMB treatment and there was a trend towards poorer survival after the introduction of EMB ($n=2$–4 batches of independent experiments). All quantitative data are presented as means ± SEM and were analyzed by two-way ANOVA (*$p<0.05$, **$p<0.01$, ***$p<0.001$, ****$p<0.0001$)

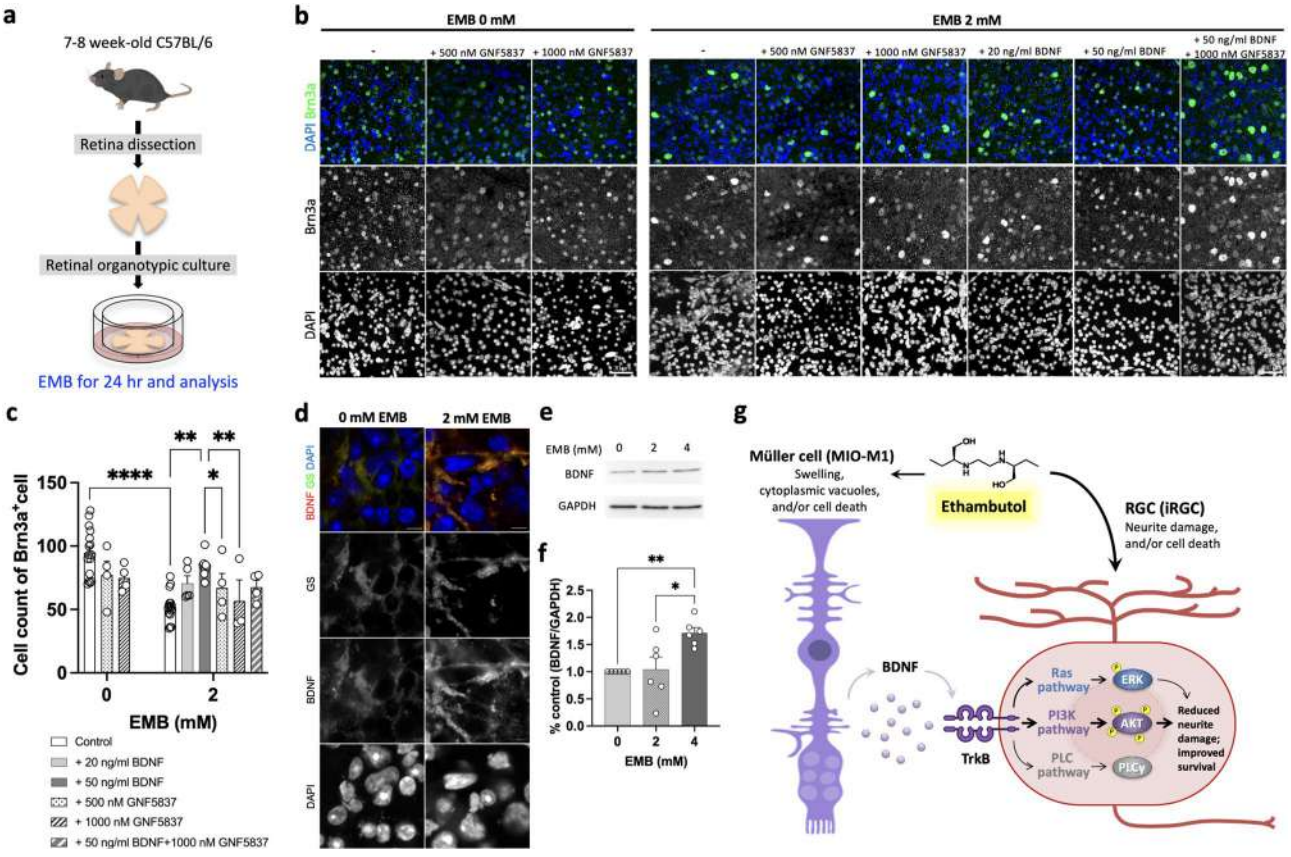


Fig. 6 The effect of BDNF on RGCs in mouse retinal organotypic culture under EMB toxicity. **a** The experimental workflow used to assess EMB-induced toxicity in mouse retinal explants. **b** Retinal flat-mount immunostaining showed that the number of Brn3a$^+$ cells increase after BDNF treatment (50 ng/ml) in the presence of 2 mM EMB, compared to retina exposed to 2 mM EMB alone. Scale bar, 30 µm. **c** Quantification of Brn3a$^+$ cells showed significant increase after adding 50 ng/ml BDNF under 2 mM EMB, and this effect was partially suppressed by GNF-5837. The calculated cell counts were averaged from five regions of 150 µm x150 µm per sample. Data are presented as means ± SEM. ($n = 3$–16 batches of independent experiments; *$p < 0.05$, **$p < 0.01$, ****$p < 0.0001$ by two-way ANOVA). **d** Retinal flat-mount immunostaining showed increased BDNF fluorescence after 2 mM EMB treatment. The BDNF was co-localized with glutamine synthetase (GS), which implies that the BDNF is present in Müller cells. Scale bar, 5 µm. **e** Western blot analysis of BDNF protein levels in mouse retina. **f** Quantification of (**e**) showing a significant increase in BDNF protein levels in mouse retina treated with 4 mM EMB compared to control (0 mM EMB). Data are presented as means ± SEM. ($n = 6$ batches of independent experiments; *$p < 0.5$, **$p < 0.01$ by one-way ANOVA). **g** Proposed mechanisms for EMB-induced optic neuropathy and the relevant neuroprotection pathways from the perspective of Müller cells. When exposed to a low (non-lethal) dose of EMB, MIO-M1 cells secrete BDNF, which activates the TrkB receptor on iRGCs. This predominantly initiates the PI3K/AKT signaling pathways and, to a lesser extent, the RAS/ERK signaling pathway. The convergence of these pathways results in reduced neurite damage and improved iRGC survival, suggesting a neuroprotective mechanism whereby EMB-induced damage is mitigated

this was not statistically significant (Fig. 5b and d). A similar trend was observed for ERK44 (Fig. 5b and e). No significant changes or trends for PLCγ1 were observed after treatment with EMB and/or BDNF (Fig. 5b and f). Together, these findings suggest that BDNF promotes survival of RGCs via AKT.

BDNF-Trk has been demonstrated to promote cell survival via a number of different downstream signaling molecules, including the AKT, ERK and PLCγ pathways [22]. The alamarBlue® assay showed similar results whereby BDNF improved the survival of iRGCs at various concentrations of EMB. This protective effect of BDNF was abolished by GNF-5837, was partially suppressed by MK-2206, an AKT inhibitor, and was not influenced by GDC-0094, an ERK inhibitor. On the other hand, GNF-5837 and MK-2206 showed similar suppression effects on the survival benefit obtained from BDNF in iRGCs without EMB treatment. Adding MK-2206 itself results in a significant impact on iRGCs without EMB treatment and a deleterious trend after the use of EMB (Fig. 5g).

Beneficial effect of BDNF on the survival of RGCs in the presence of EMB toxicity

To validate our in vitro findings, we used mouse retinal organotypic culture as our model and Brn3 as a marker for RGCs (Fig. 6a). The number of Brn3a-positive cells decreased as the EMB concentration increased and this occurred in a dose-dependent manner (Figure S4); this demonstrates that EMB-induced optic neuropathy occurs

in our retinal organotypic culture model. Treatment of BDNF (50 ng/mL) significantly increased the number of Brn3a-positive cells in retinal explants exposed to 2 mM EMB. The pro-survival effect of BDNF was suppressed by GNF-5837 (Fig. 6b and c), demonstrating that the positive effect of BDNF on RGCs is Trk receptor-dependent.

Detection of BDNF in Müller glia of the mouse retina

We have shown that treatment of EMB induces expression of BDNF in MIO-M1 cells (Fig. 4). Next, we detected BDNF by immunostaining of retinal flat mounts. BDNF was present in the cytoplasm of glutamine synthetase (GS)-positive Müller cells. Furthermore, the intensity of BDNF immunofluorescence increased in the presence of EMB and the BDNF protein levels also increased as the EMB concentration increased (Fig. 6d-f). These findings support our hypothesis that EMB induces a neuroprotective response in Müller cells by upregulating BDNF, which may contribute to RGC survival under EMB-induced stress.

Discussion

In this study, we demonstrated that EMB significantly disrupts neurotrophin signaling in human iRGCs, particularly at the level of BDNF-associated downstream pathways, as revealed by RNA sequencing and functional analyses. Importantly, iRGCs co-cultured with MIO-M1 cells show a significantly improved iRGC survival. With the support of the survival benefit created by co-culture with MIO-M1 cells, we have been able to show that BDNF expressed by MIO-M1 cells acts as a pro-survival factor when iRGCs are treated with EMB. We have also confirmed that BDNF has a protective role when mouse retinal explants are treated with EMB. Administration of BDNF improved the survival of RGCs in our organotypic culture system and this effect can be suppressed by GNF-5837, a pan-TRK inhibitor. In addition, an elevated level of BDNF protein was noted in the MIO-M1 cells line and in Müller cells present in the mouse retina. Furthermore, we found that, among the three BDNF-associated signaling molecules, AKT is the most strongly activated when BDNF is added to EMB-treated iRGCs; this increase is significantly greater than that of ERK or PLCγ1 under the same conditions. These findings are supported by the iRGCs survival experiments where either GNF-5837 (a pan-TRK inhibitor) or MK-2206 (an AKT inhibitor) are present; their presence is able to suppress the protective effect of BDNF on EMB-treated iRGCs. Together, our results support the hypothesis that BDNF protects RGC from EMB toxicity and that in these circumstances AKT acts as the major downstream signaling molecule (Fig. 6g).

Müller cells are one of the major glia populations in the mammalian retina; they span the entire retina and support various essential functions of their surrounding neurons [14]. Studies have shown that Müller cells are able to become reactive when pathological conditions are present, which results in these cells releasing inflammatory and growth factors. In these circumstances glial scars may be formed resulting in an extreme pathological state [9, 23, 24]. Whether Müller cells are beneficial or detrimental to the survival of RGCs and axon regeneration by RGCs seems to be a dynamic process. There seems to be a balance whereby, in certain circumstances, the process may lead to scar formation [9, 23, 24]. In this study, we investigated the effect of EMB toxicity on MIO-M1 cells. Although the cell number of MIO-M1 cells did not decrease significantly until 16 mM EMB treatment was reached, various progressive morphological changes were able to be observed before this concentration. These include cellular hypertrophy and increased numbers of vacuoles in the cytosol of the MIO-M1 cells. Similar cytoplasmic vacuolar changes have also been observed in Thy-1(+) ganglion neurons present in the retina of Sprague–Dawley rats [25]. These cytoplasmic vacuoles were later found to be lysosomes containing high levels of zinc, which implies that EMB induces zinc toxicity and lysosomal dysfunction may be a universal response across various different cell types [7, 26]. In the transwell co-culture system, we found that when iRGCs co-cultured with MIO-M1 cells, this results in an improved survival when EMB toxicity is present. Adding fresh medium to the system showed that there was a trend towards improved iRGC survival but that this was not as great as when the cells are co-cultured with MIO-M1 cells. Garcia et al. have also found that secretary factors from the Müller cells of adult porcine retina improves the survival of cultured porcine RGCs and that the addition of BDNF or Müller cells as a substrate seems to improve the morphology of RGCs [27].

We also showed that both BDNF mRNA and NGF mRNA were elevated in EMB-treated MIO-M1 cells. Both BDNF and NGF are neurotrophins, which is a group of closely related proteins that control many aspects of the survival, development, differentiation and functioning of neurons [28]. Neurotrophins had been widely studied in the context of neuroprotection. In the field of visual neuroscience, studies had shown that neurotrophins are able to increase numbers in optic nerve head astrocytes and lamina cribrosa cells [29, 30]. In an animal model involving optic nerve crush, recombinant human NGF (rhNGF) has been shown to promote neural regeneration [31]. In a rat glaucoma model, it has been shown that multiple neurotrophins not only contribute to pro-survival, but also help pro-apoptotic signaling; this suggests that a dynamic inter-relationships are present [32]. Another study has shown that magnetic

nanoparticles-conjugated NGF and BDNF are able to prevent RGC loss when it is induced by oxidative stress [33].

In our study, we found that BDNF alone is able to improve the survival of iRGCs under EMB toxicity. Although BDNF mRNA levels in iRGCs do not change significantly after EMB treatment, we observe a marked downregulation of NTRK2 (TrkB), the primary BDNF receptor. Moreover, IPA and Western blot analyses reveal impaired activation of downstream BDNF signaling components, particularly AKT, ERK, and PLCγ1, following EMB treatment. Therefore, we concluded that EMB disrupts BDNF-associated signaling primarily at the receptor and post-receptor signaling levels, rather than at the ligand expression level. Our findings suggested that BDNF is one of the major protective factors that contributed to the survival benefit observed in iRGCs co-cultured with Müller cells. Our subsequent experiments also support the protective effect of BDNF when an EMB-treated mouse retina explant model is used and we have confirmed that an elevation in BDNF protein level occurs in both MIO-M1 cells and in mouse retina explants. BDNF is widely expressed in the mammalian brain and exerts its pro-survival benefits by binding to the tropomyosin receptor kinase B (TrkB) receptor, which is also abundant in retinal ganglion cells and Müller glia cells [34–36]. After binding with BDNF, TrkB initiates dimerization and autophosphorylation, which is followed by activation of various signaling pathways including the phosphatidylinositol 3-kinase (PI3K)/Akt, the ERK, and the PLC-γ-dependent pathways [37]. In our study, the Akt pathway is activated to the greatest level when adding BDNF to EMB-treated iRGCs; the activation of the ERK and PLCγ1 pathways occurs to a much lower degree. From the literature, it can be seen that the PI3K/Akt-related pathway is able to exert antiapoptotic and pro-survival activities, is able to modulate N-methyl-D-aspartate (NMDA) receptor-dependent synaptic plasticity, and is able to enhance dendritic growth/branching [38–40]. All of the above may contribute to improved cell survival and help to overcome the neurotoxicity of EMB.

It has been reported that 20–50% of patients with severe EMB-related optic neuropathy had persistent visual impairment despite prompt cessation of EMB [41–43]. The reported pooled cumulative incidence of permanent impairment was 2.3–4.3/1000 persons [2]. In one cohort, the average estimated time for visual recovery was 15.2 months, with 50% of patients recovering vision by 8.3 months after discontinuing EMB [42]. Based on these findings, there is a significant number of patients suffering from persistent visual loss or the long process of visual recovery from EMB-related optic neuropathy. BDNF associated pathway may serve as a therapeutic candidate to improve the visual function or fasten the visual recovery.

This study used iRGCs derived from human iPSCs in our in vitro RGC model in order to study EMB-associated optic neuropathy. These reprogrammed iRGCs have been shown to express a range of RGC-specific markers and to show stimulus-induced channel activity, namely the cell shows electrical properties [16]. We believed that iRGCs are able to simulate the response of human RGCs that have suffered the toxic effects of EMB and that there is the possibility that this could lead to clinical applications. We verified our results using an adult mouse retinal organotypic culture system. This retinal explant culture system has been widely used and allows a preservation of the interaction between the multiplicity of cell types within the neuroretina [18, 44]. In addition, retinal explant cultures offer an ethical alternative to in vivo experiments by reducing animal distress and lowering the number of animals needed by enabling use of both retinas for pair-wise comparisons [44].

It is well-established that Müller cells can secret multiple neurotrophic factors, including BDNF, NGF, IGF-1, bFGF, CNTF, pigment epithelium-derived factor (PEDF), glial cell derived neurotrophic factor (GDNF), and so on [45, 46]. In the current study, we highlighted that BDNF plays a pivotal role in EMB-related toxicity. It will be worth investigating other potential neurotrophic factors as adjuvant or sequential agents to treat EMB-related neuronal toxicity and their interactions, which may help the understanding of Müller glia's full protective capacity in the future.

Conclusions

In this study, we first analyzed the molecular response of iRGCs to EMB treatment using RNA sequencing and found that neurotrophin signaling was significantly dysregulated. Co-culture of Müller cells with iRGCs result in improved iRGC survival when EMB toxicity is present, likely due to the secretion of BDNF by Müller cells. We have further shown that adding BDNF is able to improve the survival of iRGCs and of RGCs in a retinal organotypic culture system. The survival benefit brought about by BDNF seem to occur via the AKT pathway. These findings provide a foundation for Müller glia-associated neuroprotection during EMB-related optic neuropathy. Our findings highlight the importance of the BDNF-TrkB-AKT pathway and shows that the pathway should be investigated further in order to develop an improved treatment strategy for EMB-associated neurotoxicity.

Abbreviations

AraC	Arabinofuranosyl cytidine
BDNF	Brain-derived neurotrophic factor
bFGF	Basic fibroblast growth factor
CNTF	Ciliary neurotrophic factor

CO_2	Carbon dioxide
DAPI	4′,6-diamidino-2-phenylindole
DEGs	Differentially expressed genes
DMEM	Dulbecco's Modified Eagle Medium
EMB	Ethambutol
ERK	Extracellular signal-regulated kinase
EthD-1	Ethidium homodimer-1
FBS	Fetal bovine serum
hiPSCs	Human induced pluripotent stem cells
HRP	Horseradish peroxidase
IACUC	Institutional Animal Care and Use Committee
IGF-1	Insulin-like growth factor 1
IPA	Ingenuity Pathway Analysis (IPA)
iRGCs	HiPSC-derived retinal ganglion cell-like cells
MIO-M1	Moorfields/Institute of Ophthalmology- Müller 1
NGF	Human nerve growth factor
PBS	Phosphate-buffered saline
PCA	Principal component analysis
PI3K	Phosphatidylinositol 3-kinase
PLC-γ	Phospholipase C-γ
quantitative RT-PCR	Real-time quantitative PCR
TBP	TATA-box binding protein
TEPC	Track-etched polycarbonate membrane
TrkB	Tropomyosin receptor kinase B

Supplementary Information

The online version contains supplementary material available at https://doi.org/10.1186/s12964-025-02478-4.

Supplementary Material 1.

Supplementary Material 2.

Acknowledgements
We thank Ya-Han Chang for helping with sample preparation, immunocytochemistry and technical support, and Yu-Yang Chen for support with image acquisition. We also acknowledge the Human Disease iPSC Service Consortium funded by the NSTC (112-2740-B-001-004) for iPSC generation and technical support. This work was partially supported by the Brain Research Center of National Yang Ming Chiao Tung University from The Featured Areas Research Center Program within the framework of the Higher Education Sprout Project by the Ministry of Education (MOE) in Taiwan.

Authors' contributions
H.C.C, Y.H.W and J.Y.Y. performed study concept and design; H.C.C, Y.H.W, A.G.W. and J.Y.Y. performed development of methodology and writing, review and revision of the paper; H.C.C, Y.H.W, Y.L.Y., H.C.J., R.H.C.L., A.G.W. and J.Y.Y. provided acquisition, analysis and interpretation of data, and statistical analysis; S.W.C. performed bioinformatics analysis; Y.H.W, Y.L.Y., H.C.J., R.H.C.L., and J.Y.Y. provided technical and material support. All authors read and approved the final manuscript.

Funding
This study was supported by Taipei Veterans General Hospital (grant no. VGH V112C-069), National Science and Technology Council of Taiwan (grant no. MOST 110-2314-B-075-054-MY3, NSTC 114-2628-B-075-003-MY3 and NSTC 112-2311-B-A49 -003) and Yen Tjing Ling Medical Foundation (CI-113-28).

Data availability
RNA sequencing data have been deposited in the NCBI Gene Expression Omnibus under accession number GSE294687 and will be made publicly available upon publication of the accepted article. Materials and other datasets used and/or analyzed during the current study are available from the corresponding author upon reasonable request.

Declarations

Ethics approval and consent to participate
All procedures regarding animal handling and euthanizing complied with the ARVO Statement for the Use of Animals in Ophthalmic and Vision Research and were approved by the Institutional Animal Care and Use Committee (IACUC) of Taipei Veterans General Hospital (#2020 – 272) and of National Yang Ming Chiao Tung University (#1111006). The use of hiPSC lines followed the Policy Instructions of the Ethics of Human Embryo and Embryonic Stem Cell Research guidelines in Taiwan. Approval from the Institutional Review Boards of National Yang Ming Chiao Tung University was obtained (# NYCU112122AW).

Consent for publication
Not applicable.

Competing interests
The authors declare no competing interests.

Author details
[1]Department of Ophthalmology, Taipei Veterans General Hospital, Taipei, Taiwan
[2]Department of Ophthalmology, School of Medicine, National Yang Ming Chiao Tung University, Taipei, Taiwan
[3]Brain Research Center, National Yang Ming Chiao Tung University, Taipei, Taiwan
[4]Department of Life Sciences and Institute of Genome Sciences, College of Life Sciences, National Yang Ming Chiao Tung University, Taipei, Taiwan
[5]Department of Internal Medicine, College of Medicine, National Taiwan University, Taipei, Taiwan

Received: 16 April 2025 / Accepted: 6 October 2025
Published online: 03 November 2025

References

1. Sadun AA, Wang MY. Ethambutol optic neuropathy: how we can prevent 100,000 new cases of blindness each year. J Neuroophthalmol. 2008;28:265–8.
2. Ezer N, Benedetti A, Darvish-Zargar M, Menzies D. Incidence of ethambutol-related visual impairment during treatment of active tuberculosis. Int J Tuberc Lung Dis. 2013;17:447–55.
3. Talbert Estlin KA, Sadun AA. Risk factors for ethambutol optic toxicity. Int Ophthalmol. 2010;30:63–72.
4. Chamberlain PD, Sadaka A, Berry S, Lee AG. Ethambutol optic neuropathy. Curr Opin Ophthalmol. 2017;28:545–51.
5. Kozak SF, Inderlied CB, Hsu HY, Heller KB, Sadun AA. The role of copper on ethambutol's antimicrobial action and implications for ethambutol-induced optic neuropathy. Diagn Microbiol Infect Dis. 1998;30:83–7.
6. Wang MY, Sadun AA. Drug-related mitochondrial optic neuropathies. J Neuroophthalmol. 2013;33:172–8.
7. Chung H, Yoon YH, Hwang JJ, Cho KS, Koh JY, Kim JG. Ethambutol-induced toxicity is mediated by zinc and lysosomal membrane permeabilization in cultured retinal cells. Toxicol Appl Pharmacol. 2009;235:163–70.
8. Huang SP, Chien JY, Tsai RK. Ethambutol induces impaired autophagic flux and apoptosis in the rat retina. Dis Model Mech. 2015;8:977–87.
9. Vecino E, Rodriguez FD, Ruzafa N, Pereiro X, Sharma SC. Glia-neuron interactions in the mammalian retina. Prog Retin Eye Res. 2016;51:1–40.
10. Rogers RS, Dharsee M, Ackloo S, Sivak JM, Flanagan JG. Proteomics analyses of human optic nerve head astrocytes following biomechanical strain. Mol Cell Proteomics. 2012;11:M111012302.
11. Ma W, Zhao L, Fontainhas AM, Fariss RN, Wong WT. Microglia in the mouse retina alter the structure and function of retinal pigmented epithelial cells: a potential cellular interaction relevant to AMD. PLoS ONE. 2009;4:e7945.
12. Langmann T. Microglia activation in retinal degeneration. J Leukoc Biol. 2007;81:1345–51.
13. Bringmann A, Pannicke T, Grosche J, Francke M, Wiedemann P, Skatchkov SN, et al. Muller cells in the healthy and diseased retina. Prog Retin Eye Res. 2006;25:397–424.
14. Reichenbach A, Bringmann A. Glia of the human retina. Glia. 2020;68:768–96.
15. Bringmann A, Iandiev I, Pannicke T, Wurm A, Hollborn M, Wiedemann P, et al. Cellular signaling and factors involved in Muller cell gliosis: neuroprotective and detrimental effects. Prog Retin Eye Res. 2009;28:423–51.
16. Liou RH, Chen SW, Cheng HC, Wu PC, Chang YF, Wang AG, et al. The efficient induction of human retinal ganglion-like cells provides a platform for studying optic neuropathies. Cell Mol Life Sci. 2023;80:239.

17. Limb GA, Salt TE, Munro PM, Moss SE, Khaw PT. In vitro characterization of a spontaneously immortalized human Muller cell line (MIO-M1). Invest Ophthalmol Vis Sci. 2002;43:864–9.
18. Muller B, Wagner F, Lorenz B, Stieger K. Organotypic cultures of adult mouse retina: morphologic changes and gene expression. Invest Ophthalmol Vis Sci. 2017;58:1930–40.
19. Ho SY, Chao CY, Huang HL, Chiu TW, Charoenkwan P, Hwang E. Neurphologyj: an automatic neuronal morphology quantification method and its application in pharmacological discovery. BMC Bioinformatics. 2011;12:230.
20. Bessero AC, Clarke PG. Neuroprotection for optic nerve disorders. Curr Opin Neurol. 2010;23:10–5.
21. Vogel C, Marcotte EM. Insights into the regulation of protein abundance from proteomic and transcriptomic analyses. Nat Rev Genet. 2012;13:227–32.
22. Bathina S, Das UN. Brain-derived neurotrophic factor and its clinical implications. Arch Med Sci. 2015;11:1164–78.
23. Miao Y, Zhao GL, Cheng S, Wang Z, Yang XL. Activation of retinal glial cells contributes to the degeneration of ganglion cells in experimental glaucoma. Prog Retin Eye Res. 2023;93:101169.
24. Yoo HS, Shanmugalingam U, Smith PD. Harnessing astrocytes and muller glial cells in the retina for survival and regeneration of retinal ganglion cells. Cells. 2021. https://doi.org/10.3390/cells10061339.
25. Yoon YH, Jung KH, Sadun AA, Shin HC, Koh JY. Ethambutol-induced vacuolar changes and neuronal loss in rat retinal cell culture: mediation by endogenous zinc. Toxicol Appl Pharmacol. 2000;162:107–14.
26. Yamada D, Saiki S, Furuya N, Ishikawa K, Imamichi Y, Kambe T, et al. Ethambutol neutralizes lysosomes and causes lysosomal zinc accumulation. Biochem Biophys Res Commun. 2016;471:109–16.
27. Garcia M, Forster V, Hicks D, Vecino E. Effects of Muller glia on cell survival and neuritogenesis in adult Porcine retina in vitro. Invest Ophthalmol Vis Sci. 2002;43:3735–43.
28. Skaper SD. The neurotrophin family of neurotrophic factors: an overview. Methods Mol Biol. 2012;846:1–12.
29. Lambert WS, Clark AF, Wordinger RJ. Effect of exogenous neurotrophins on Trk receptor phosphorylation, cell proliferation, and neurotrophin secretion by cells isolated from the human lamina cribrosa. Mol Vis. 2004;10:289–96.
30. Lambert WS, Clark AF, Wordinger RJ. Neurotrophin and Trk expression by cells of the human lamina cribrosa following oxygen-glucose deprivation. BMC Neurosci. 2004;5(1):51.
31. Mesentier-Louro LA, Rosso P, Carito V, Mendez-Otero R, Santiago MF, Rama P, et al. Nerve growth factor role on retinal ganglion cell survival and axon regrowth: effects of ocular administration in experimental model of optic nerve injury. Mol Neurobiol. 2019;56:1056–69.
32. Johnson EC, Guo Y, Cepurna WO. Neurotrophin roles in retinal ganglion cell survival: lessons from rat glaucoma models. Exp Eye Res. 2009;88:808–15.
33. Giannaccini M, Usai A, Chiellini F, Guadagni V, Andreazzoli M, Ori M, et al. Neurotrophin-conjugated nanoparticles prevent retina damage induced by oxidative stress. Cell Mol Life Sci. 2018;75:1255–67.
34. Wahlin KJ, Campochiaro PA, Zack DJ, Adler R. Neurotrophic factors cause activation of intracellular signaling pathways in Muller cells and other cells of the inner retina, but not photoreceptors. Invest Ophthalmol Vis Sci. 2000;41:927–36.
35. Pease ME, McKinnon SJ, Quigley HA, Kerrigan-Baumrind LA, Zack DJ. Obstructed axonal transport of BDNF and its receptor TrkB in experimental glaucoma. Invest Ophthalmol Vis Sci. 2000;41:764–74.
36. Grishanin RN, Yang H, Liu X, Donohue-Rolfe K, Nune GC, Zang K, et al. Retinal TrkB receptors regulate neural development in the inner, but not outer, retina. Mol Cell Neurosci. 2008;38:431–43.
37. Numakawa T, Suzuki S, Kumamaru E, Adachi N, Richards M, Kunugi H. Bdnf function and intracellular signaling in neurons. Histol Histopathol. 2010;25:237–58.
38. Baydyuk M, Xu B. BDNF signaling and survival of striatal neurons. Front Cell Neurosci. 2014;8:254.
39. Park H, Poo MM. Neurotrophin regulation of neural circuit development and function. Nat Rev Neurosci. 2013;14:7–23.
40. Jaworski J, Spangler S, Seeburg DP, Hoogenraad CC, Sheng M. Control of dendritic arborization by the phosphoinositide-3'-kinase-Akt-mammalian target of rapamycin pathway. J Neurosci. 2005;25:11300–12.
41. Tsai RK, Lee YH. Reversibility of ethambutol optic neuropathy. J Ocul Pharmacol Ther. 1997;13:473–7.
42. An HR, Lee BJ, Moon Y. Visual recovery time in patients with Ethambutol-induced toxic optic neuropathy. Korean J Ophthalmol. 2024;38:91–7.
43. Chen SC, Lin MC, Sheu SJ. Incidence and prognostic factor of ethambutol-related optic neuropathy: 10-year experience in Southern Taiwan. Kaohsiung J Med Sci. 2015;31:358–62.
44. Schnichels S, Paquet-Durand F, Loscher M, Tsai T, Hurst J, Joachim SC, et al. Retina in a dish: cell cultures, retinal explants and animal models for common diseases of the retina. Prog Retin Eye Res. 2021;81:100880.
45. Eastlake K, Lamb WDB, Luis J, Khaw PT, Jayaram H, Limb GA. Prospects for the application of Muller glia and their derivatives in retinal regenerative therapies. Prog Retin Eye Res. 2021;85:100970.
46. Arrigo A, Cremona O, Aragona E, Casoni F, Consalez G, Dogru RM, Hauck SM, Antropoli A, Bianco L, Parodi MB, et al. Muller cells trophism and pathology as the next therapeutic targets for retinal diseases. Prog Retin Eye Res. 2025;106:101357.

Publisher's Note

Springer Nature remains neutral with regard to jurisdictional claims in published maps and institutional affiliations.